Particle discrimination in a NaI crystal using the COSINUS remote TES design

G. Angloher,[1] M. R. Bharadwaj,[1] I. Dafinei,[2,3] N. Di Marco,[2,4] L. Einfalt,[5,6] F. Ferroni,[3,2] S. Fichtinger,[5] A. Filipponi,[7,4] T. Frank,[1] M. Friedl,[5] A. Fuss,[5,6] Z. Ge,[8] M. Heikinheimo,[9] M. N. Hughes,[1] K. Huitu,[9] M. Kellermann,[1] R. Maji,[5,6] M. Mancuso,[1] L. Pagnanini,[2,4] F. Petricca,[1] S. Pirro,[4] F. Pröbst,[1] G. Profeta,[7,4] A. Puiu,[2,4] F. Reindl,[5,6] K. Schäffner,[1] J. Schieck,[5,6] D. Schmiedmayer,[5,6] C. Schwertner,[5,6] M. Stahlberg,[1,*] A. Stendahl,[9] M. Stukel,[2,4] C. Tresca,[7,4] F. Wagner,[5] S. Yue,[8] V. Zema,[1,†] Y. Zhu,[8]

(COSINUS Collaboration)

A. Bento,[10,1] L. Canonica,[1] and A. Garai[1]

[1]*Max-Planck-Institut für Physik, 80805 München—Germany*
[2]*Gran Sasso Science Institute, 67100 L'Aquila—Italy*
[3]*INFN—Sezione di Roma, 00185 Roma—Italy*
[4]*INFN—Laboratori Nazionali del Gran Sasso, 67100 L'Aquila—Italy*
[5]*Institut für Hochenergiephysik der Österreichischen Akademie der Wissenschaften, 1050 Wien—Austria*
[6]*Atominstitut, Technische Universität Wien, 1020 Wien—Austria*
[7]*Dipartimento di Scienze Fisiche e Chimiche, Università degli Studi dell'Aquila, 67100 L'Aquila—Italy*
[8]*SICCAS—Shanghai Institute of Ceramics, Shanghai—P.R.China 201899*
[9]*Helsinki Institute of Physics, University of Helsinki, 00014 Helsinki—Finland*
[10]*LIBPhys-UC, Physics Departments, University of Coimbra, 3004-516 Coimbra—Portugal*

(Received 30 June 2023; revised 16 January 2024; accepted 23 February 2024; published 29 April 2024; corrected 12 July 2024)

The COSINUS direct dark matter experiment situated at Laboratori Nazionali del Gran Sasso in Italy is set to investigate the nature of the annually modulating signal detected by the DAMA/LIBRA experiment. COSINUS has already demonstrated that sodium iodide crystals can be operated at mK temperature as cryogenic scintillating calorimeters using transition edge sensors, despite the complication of handling a hygroscopic and low melting point material. With results from a new COSINUS prototype, we show that particle discrimination on an event-by-event basis in NaI is feasible using the dual-channel readout of both phonons and scintillation light. The detector was mounted in the novel remoTES design and operated in an above-ground facility for 9.06 g · d of exposure. With a 3.7 g NaI crystal, e^-/γ events could be clearly distinguished from nuclear recoils down to the nuclear recoil energy threshold of 20 keV.

DOI: 10.1103/PhysRevD.109.082003

I. INTRODUCTION

In the field of direct dark matter searches null results have been reported by most experiments [1] with the notable exception of DAMA/LIBRA [2]. DAMA/LIBRA measures scintillation light created by particle interactions in NaI target crystals at room temperature. An annual modulation of the recorded event rate has been observed for many years, which is consistent with particle interactions, but incompatible with results from other direct searches in this interpretation [1]. The origin of the signal remains unclear. Several experiments have set out to study this phenomenon using the same target material, and strong constraints on the modulation amplitude have been reported by COSINE-100 [3] and ANAIS [4], which follow a similar detection principle as DAMA/LIBRA. Among the NaI experiments, Cryogenic Observatory for SIgnals seen in Next generation Underground Searches (COSINUS) will be the only one to feature a direct measurement of the nuclear recoil energy per event. This is of crucial importance to solve the uncertainty on the light quenching factors for recoils off Na and I which affects the interpretation of data collected with single channel scintillators in the dark matter-nucleus interaction scenario, see e.g., [5–10]. The measurement of

*Corresponding author: martin.stahlberg@mpp.mpg.de
†Corresponding author: vanessa.zema@mpp.mpg.de

Published by the American Physical Society under the terms of the Creative Commons Attribution 4.0 International license. Further distribution of this work must maintain attribution to the author(s) and the published article's title, journal citation, and DOI. Open access publication funded by the Max Planck Society.

the true nuclear recoil energy is possible through the use of transition edge sensors (TES) which are coupled to the NaI target crystals to provide another channel in addition to the scintillation light. NaI poses certain difficulties when operated in this calorimetric approach, such as hygroscopicity and a low melting point [11]. A solution to this problem is the remoTES design, where the TES sensor is deposited on a separate wafer, which is then coupled to the absorber crystal using a Au wire and pad [12]. The first results of this coupling scheme for detectors with Si and TeO_2 absorbers were described in Ref. [12]. We demonstrate in this work that the same principle is applicable to NaI crystals, and present results from the first NaI-remoTES detector. In particular, we show that discrimination between e^-/γ events and nuclear recoils on an event-by-event basis is possible in NaI, which constitutes a milestone for COSINUS. In the next step, COSINUS will scale up the NaI absorber mass. With 100 kg · days of total exposure, COSINUS will probe a first set of dark matter models compatible with DAMA/LIBRA's annual modulation signal. With 1000 kg · days, COSINUS will provide a complete model independent cross check [13].

II. DETECTOR MODULE

The detector module consists of a remoTES phonon detector [12] and a silicon-on-sapphire (SOS) wafer as light detector, as shown in Figs. 1–3. The absorber is a NaI crystal manufactured by the Shanghai Institute of Ceramics. A Au pad, cut from an ingot, is glued on the absorber with EPO-TEK 301-2, a two component low out-gassing epoxy resin [14]. The Au pad is coupled to the TES wafer with two Au-wire bonds, as indicated in Fig. 1. An enlarged picture of the remoTES coupling to the absorber is shown in Fig. 2(b). An ohmic heater, fabricated on a silicon pad, is glued with EPO-TEK 301-2 on the surface of the NaI-absorber to inject heater pulses into the crystal. A ^{55}Fe x-ray source with an activity of 3 mBq is taped to the copper holder facing the NaI absorber, and irradiated this latter the side as indicated in Fig. 2(a). The TES wafer is made of Al_2O_3. The TES is a thin W film and features two aluminum bonding pads for the connection to the bias circuit. The Au wires from the Au pad are bonded onto a second pad, named the Au bridge, which overlaps with the W film (see Fig. 1). A Au-thermal-link is used to connect the TES to the thermal bath. A Au heater deposited on the wafer surface, is used to inject heater pulses and thus monitor the temperature of the TES.

The light detector is a SOS wafer, equipped with a W TES which has two phonon collectors (Al/W bilayers) [15]. It is mounted on the lid of the copper holder, which is used to protect the NaI from humid air. The light detector is irradiated with a second ^{55}Fe calibration source of similar activity as the one shining on the absorber. A picture of the light detector [Fig. 3(a)] and an enlarged view of the wire bonding of its TES [Fig. 3(b)] are shown in Fig. 3. In the following, we refer to the NaI-remoTES as the phonon channel and the light detector as the light channel, interchangeably. The description of the detector components is summarized in Table I.

III. DATA TAKING

The measurement was carried out in an above-ground wet dilution refrigerator at the Max Planck Institute for Physics in Munich. The cryostat is equipped with four superconducting quantum interference devices (SQUIDs) from the APS company [16] and continuously read out with a 16-bit analog-digital converter at a sampling frequency of 50 kS/s. To reduce the background event rate induced

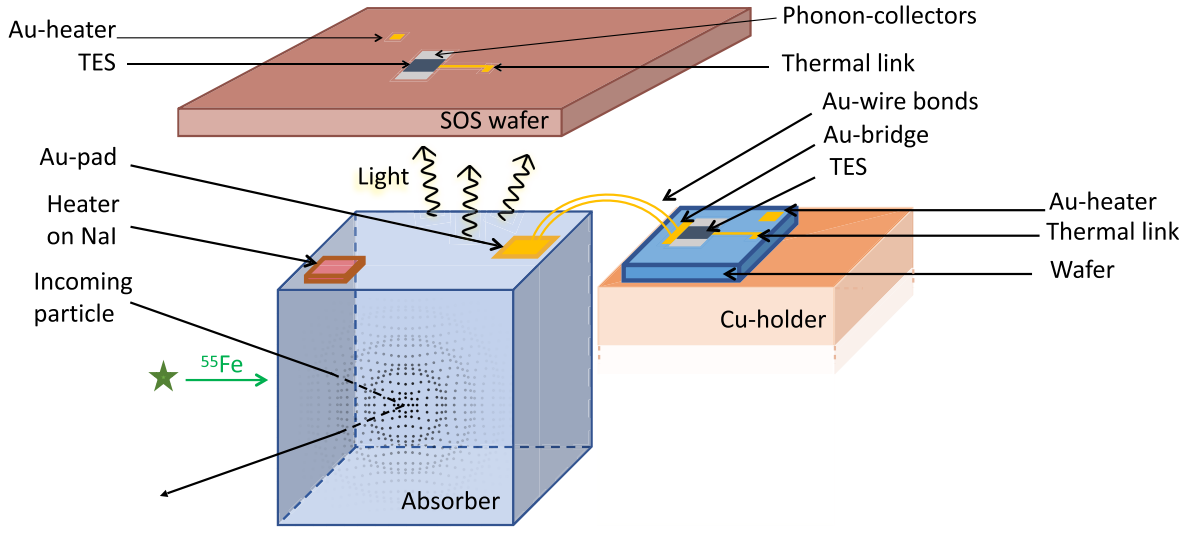

FIG. 1. Schematic of remoTES and light detector. In the remoTES, the TES is deposited on a wafer, which is separated from the absorber crystal. The coupling between the absorber and the TES consists of an Au pad glued on the absorber surface and connected to the TES by two Au-wire bonds [12]. The TES of the light detector is deposited directly on the light detector crystal surface.

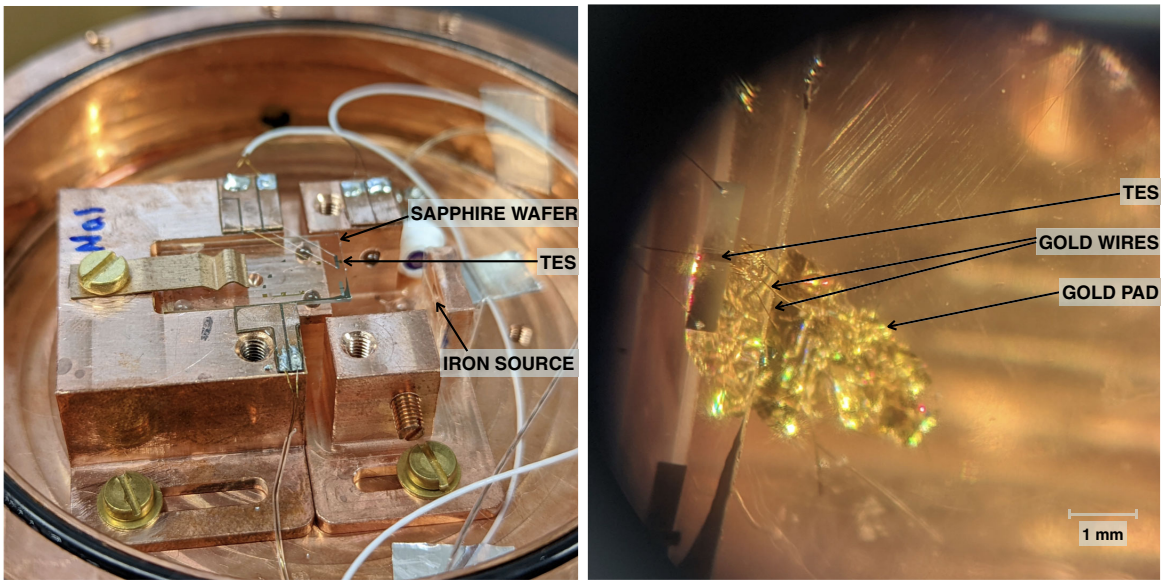

FIG. 2. (a) The remoTES wafer mounted in the copper holder. The sapphire wafer is placed on sapphire balls and held by a bronze clamp. A ^{55}Fe source is taped on a copper piece facing the absorber for the purpose of energy calibration. (b) Microscopic view of the Au pad glued on the NaI crystal and the wire bonding to the remoTES.

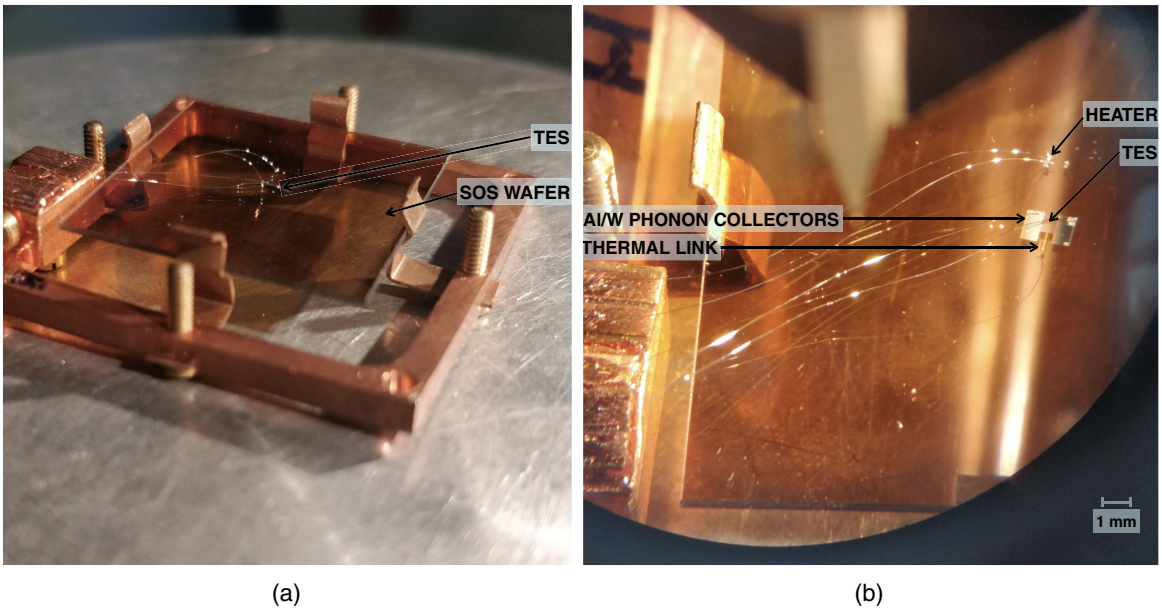

FIG. 3. (a) SOS light detector mounted in a copper holder. (b) Microscopic view of the electrical connections of the light detector TES and of its separate ohmic heater.

by cosmic and ambient radiation, a lead wall with a thickness of 10 cm was built around the refrigerator. Three subsequent datasets were recorded and are discussed in this work: a background dataset with only the (module-internal) ^{55}Fe sources present, a ^{57}Co calibration dataset, and an additional neutron calibration dataset using an AmBe source. The duration and effective exposure of each dataset are given in Table II.

IV. DATA ANALYSIS

For the three datasets discussed above, the continuous stream from the phonon channel is triggered in software using an optimal filter trigger (cf. Ref. [17] and Ref. [18]). The light channel is passively read out in parallel. The filter is created from a parametric description of the NaI channel pulse shape based on Ref. [19] and a noise power spectrum

TABLE I. Summary of phonon detector (PD) and light detector (LD) component properties. RRR: residual resistivity ratio.

Component		Properties
PD	NaI absorber	$(10 \times 10 \times 10)$ mm^3 Mass: 3.7 g
	Au pad on NaI	Area: 4 mm^2 Thickness: 1 μm RRR: ∼22
	Two Au wires	Lengths: (6.7, 10.3) mm Diameter: 17 μm
	W-TES on wafer	Area: (100×407) μm^2 Thickness: 156 nm
	Al_2O_3 wafer	$(10 \times 20 \times 1)$ mm^3
	Au heater	Area: (200×150) μm^2 Thickness: 100 nm
	Heater on NaI	Area: (3×3) mm^2 Thickness: 1 mm
	Thermal link	Resistance (300 K): 82.3 Ω
LD	SOS wafer	$(20 \times 20 \times 0.4)$ mm^3
	W-TES on SOS wafer	Area: (284×423) μm^2 Thickness: 200 nm
	Phonon collectors	Al/W bilayers Area: (526×1027) μm^2 Thickness: 1 μm

TABLE II. Measuring times, raw exposure, event rates (counts above threshold) and calibration sources for the three datasets. The dataset where only the ^{55}Fe source was present is used as a background dataset. The ^{55}Fe source is not visible in the data as it is below the energy threshold.

Measuring time (h)	Calibration sources	Event rate (cps)	Exposure (g · d)
17.73	^{55}Fe, ^{57}Co	0.57	2.73
16.40	^{55}Fe, AmBe	0.62	2.53
24.61	^{55}Fe	0.37	3.79

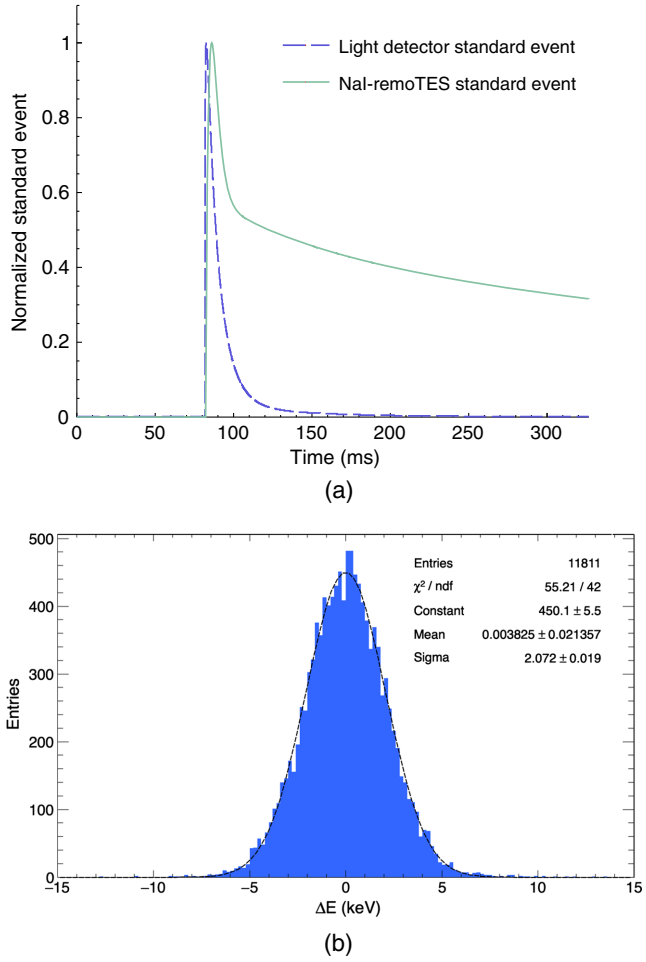

FIG. 4. (a) Normalized averaged pulses in the light detector (dashed, dark-blue curve) and in the NaI-remoTES detector (solid, water-green curve). A cleaned sample of nonsaturated events from the Co57 dataset was used for averaging. (b) Deviation of reconstructed energy from nominal energy for simulated events, obtained by superimposing scaled averaged signal pulses onto empty traces for the phonon channel.

obtained from randomly drawn empty noise traces. The typical pulse shape of absorber recoils for the NaI channel is shown in Fig. 4(a) and features a very long decay time. Both channels are calibrated using the 122 keV peak visible in the ^{57}Co dataset. The result is illustrated in 6, where also additional γ lines due to ^{57}Co are highlighted for comparison. Peaks from the ^{55}Fe source could not be observed, as their energies of 5.9 keV and 6.4 keV are below the energy threshold in both phonon and light channel. The optimum filter amplitude is used as energy estimator. In the energy range from threshold up to ∼500 keV, we see no change in the pulse shape of the phonon channel, and no saturation effects, indicating an overall linear detector performance.

A baseline energy resolution of the phonon channel of 2.07 ± 0.01 keV is determined by superimposing the pulse shape onto a set of randomly drawn empty baselines and reconstructing these artificial events. The deviation from the nominal injected energy is illustrated in Fig. 4(b). The baseline resolution of the SOS light detector for events which generate scintillation light in the absorber was determined to be 2.02 ± 0.05 keV$_{ee}$ using the same technique. All datasets were triggered in software with a threshold of 10 keV in the phonon channel.

Each dataset was cleaned by applying a set of quality cuts: Severely unstable detector operation intervals are removed by monitoring the reconstructed amplitude of injected heater pulses over time. Single voltage spike events are removed by cutting on the ratio of the numerical derivative of the pulse to the baseline rms. The rms from the optimal filter reconstruction and the rms from an additional truncated averaged pulse fit reconstruction (cf., e.g., Ref. [20]) are used to remove pile-up events and events from particle interactions in the sapphire wafer.

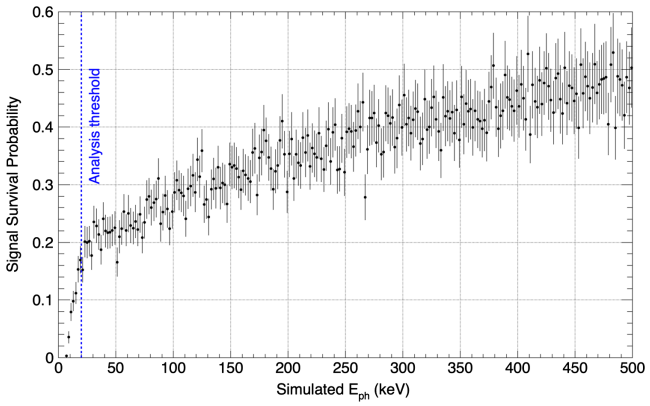

FIG. 5. Survival probability for simulated events in the analysis chain, estimated using the background dataset. An exponentially decaying energy spectrum was simulated to allow for better statistics at low energies. Statistical uncertainties are indicated for each energy bin. The analysis threshold at an efficiency of 20% is marked by a dashed blue line.

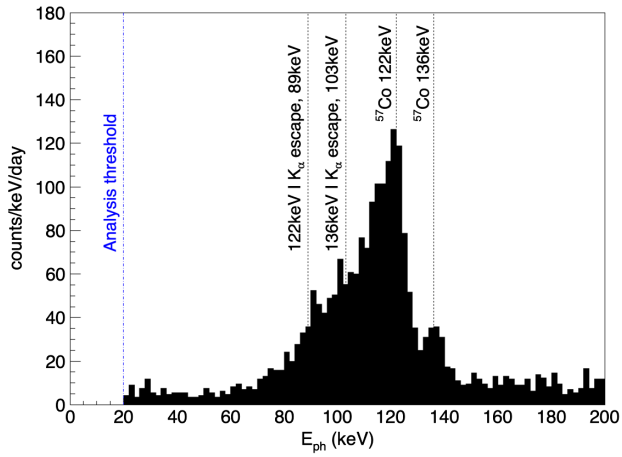

FIG. 6. Energy spectrum from the ^{57}Co γ calibration measurement. A constant conversion factor from pulse amplitude to energy was extracted by fitting a gaussian function to the right shoulder of the 122 keV, and used to calibrate the spectrum. The additional ^{57}Co 136 keV peak and two γ escape peaks due to I K-α, expected at around 88.8 keV and 102.8 keV, are used to cross check the result. The latter deviate by about 2% from their nominal value.

The effect of each quality cut is assessed by simulating pulses with an exponentially decreasing energy spectrum on the set of randomly drawn detector baselines and studying the fraction of surviving events as a function of the simulated energy. Figure 5 shows the overall survival probability for signal events in the analysis obtained from the background dataset. We find that the detector threshold of 10 keV is only nominal, i.e., only few simulated signal events survive down to this energy. This is due to varying noise conditions in the above-ground setup, very long pulse decay time resulting in pileup, and the presence of particle recoils in the wafer, which require strong quality cuts to be discarded. An analysis threshold of 20 keV is used in the following, where the signal survival probability is still about 20%. Above this threshold, no wafer-induced events or noise events are observed in the background dataset.

V. DISCRIMINATION OF NUCLEAR RECOIL BANDS

The light yield (LY) is defined as the ratio between the electron-equivalent energy measured in the light channel and the energy measured in the phonon channel for each event. It enables the discrimination of different recoil event classes. In Figs. 7 and 8 the LY is shown as a function of the phonon channel energy for the background and the neutron calibration datasets, respectively. The phonon channel energy E_{ph} is used here as an approximation of the total recoil energy per event $E_t = \eta \cdot E_L + (1-\eta) \cdot E_{ph}$, to which the light channel energy E_L only contributes a small fraction, as the scintillation efficiency η is typically on the order of a few percentages. We fit an empirical description based on [21] to the datasets in an unbinned likelihood approach, containing parameters for the combined e^-/γ band, the Na and I nuclear recoil bands, and the energy spectra in each band. The Gaussian width of the LY bands as a function of energy is given by the energy dependent resolutions of the two channels. These are described by second degree polynomials, where the constant is given by the phonon and light channel resolutions at threshold, and the remaining coefficients are fitted. The mean line of the e^-/γ band is allowed to vary linearly with phonon energy. Relative to the e^-/γ mean line $\bar{L}$, the mean lines of the Na and I bands are defined by $\bar{N}_i = Q_i \cdot \bar{L} \cdot (1-(q_{0,i} \cdot \exp(-\frac{E}{q_{1,i}})))$ with the constant quenching factors Q_{Na} and Q_I at high energies, and an exponential non-proportionality at low energies. For events in the electron band, the LY is normalized to 1 by definition, as both channels were calibrated using the 122 keV γ peak from the ^{57}Co source. The spectral description of events in the e^-/γ band consists of a constant and a linear term plus a compton scattering contribution. The compton part is empirically described as $p_0 \cdot \exp(-E \cdot p_1) \cdot (p_2 \cdot E - \frac{p_3}{E})$, where p_i are fit parameters, and originates from cosmogenic ionized particles inducing secondary electrons which in turn produce bremsstrahlung seen by the detector. Consequently, this part is assumed to be the same for neutron and background dataset, while the other contributions are determined separately for both, as the AmBe neutron source introduces additional e^-/γ background. Nuclear recoil spectra in the neutron calibration dataset are described with an exponential spectrum $p_{0,i} \cdot \exp(-\frac{E}{p_{1,i}})$ each, where $p_{0,i}$ and $p_{1,i}$ are fit parameters. A detailed motivation and description of the parametrization will be addressed in a future publication [22].

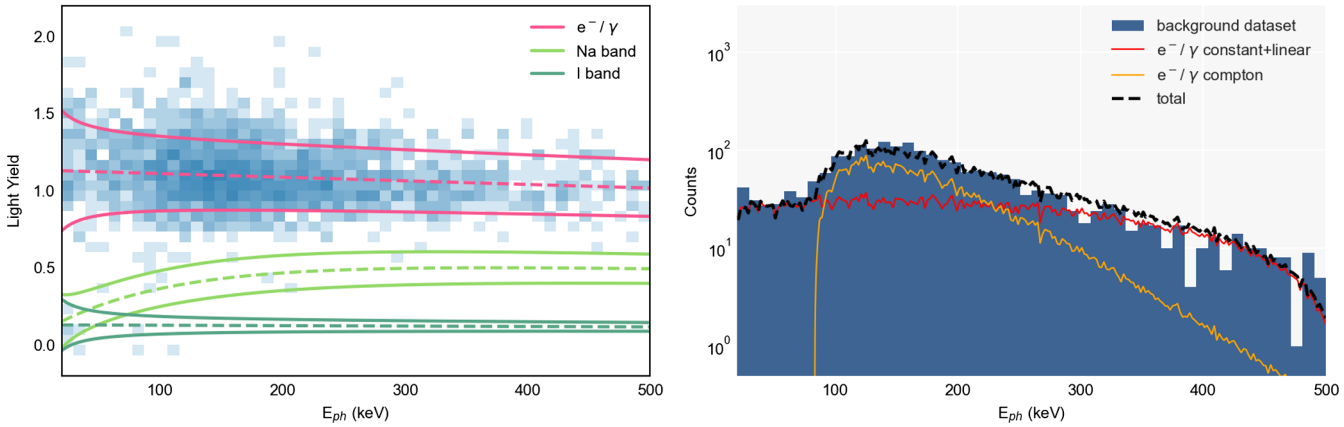

FIG. 7. Left: 2D histogram of LY versus phonon channel energy for the background dataset with color-coded number of entries. Right: e^-/γ energy spectrum of the background dataset. Different contributions are highlighted.

Figures 6 and 7 also show the result of the likelihood fit for the two datasets. 90% boundaries are drawn for the e^-/γ and Na/I nuclear recoil bands. It can be clearly seen that two new populations of events appear below the e^-/γ band in the neutron calibration dataset, far outside the 2σ boundary, which are well described by the nuclear recoil band description introduced above. In the spectrum (Fig. 7 right panel), the number of nuclear recoil events is similar to the amount of e^-/γ background events below ≈100 keV. The additional bands are quenched in LY, where the constant quenching factors are $Q_{Na} = 0.489 \pm 0.072$ and $Q_I = 0.115 \pm 0.013$, and the LY appears to be decreasing below ∼150 keV as the recoil energy approaches the threshold. In Ref. [6], a similar decline of the quenching factor in NaI at lower energies was reported for measurements at room temperature and with Tl-doped crystals. However, nonproportionality to the e^-/γ mean line at low energies may also be explained simply by a low number of scintillation photons, which results in poisson-distributed rather than gaussian-distributed LY. At increasing phonon channel energy, a slight downward tilt of the e^-/γ band is visible, which is due to increasing nonlinearity of the light detector response. A small number of nuclear recoils is also observed in the background dataset, and visible in Fig. 7. These are due to neutrons from the lead wall surrounding the cryostat. In all bands, the event density decreases at low energies due to decreasing survival probability in the analysis (cf. Fig. 5), which is accounted for in the fit. As this survival probability was obtained from the background dataset, the higher overall event rate (i.e., more dead time) in the neutron calibration data results in a small overestimation of the e^-/γ and nuclear recoil spectra in Fig. 7. The total number of events in the neutron calibration dataset is 1296, where the fit expects 1378. The background dataset contains 2118 events, 2076 of which are accounted for.

The scintillation efficiency η of the crystal could not be determined in this measurement. This parameter could be estimated from γ peaks, which should appear slightly

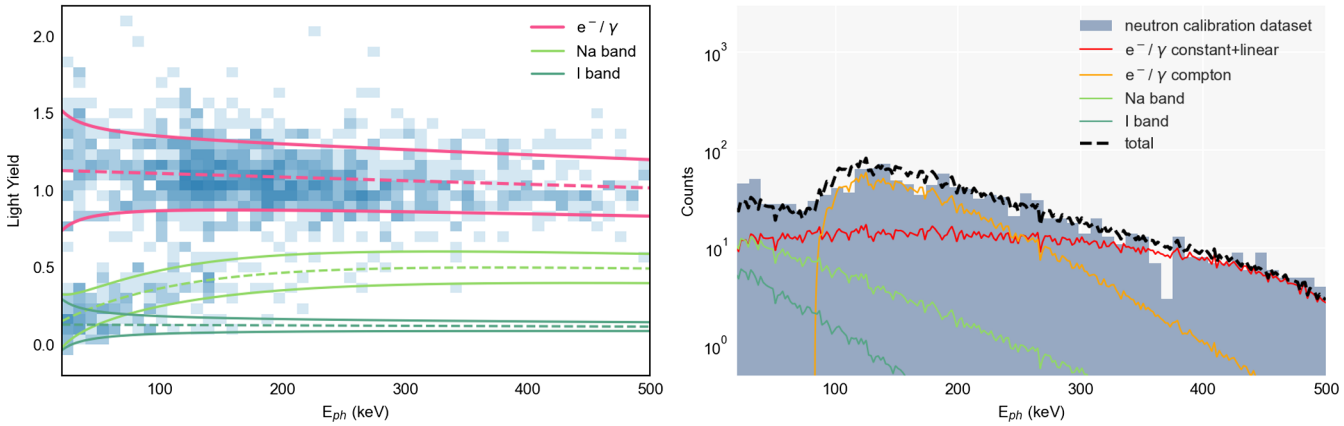

FIG. 8. Left: 2D histogram of LY versus phonon channel energy for the neutron calibration dataset with color-coded number of entries. Right: combined energy spectrum of the neutron calibration dataset. Different contributions from the recoil bands are indicated with their respective color. Additionally, the compton contribution to the e^-/γ spectrum, determined from the background dataset, is highlighted in orange.

tilted in the LY vs E_{ph} plane due to the difference between E_{ph} and E_t [23]. Unfortunately, the ^{55}Fe peaks are below threshold here, and the ^{57}Co spectrum is too complex to reliably extract this information.

In future measurements and in the final COSINUS design, particle discrimination will be further improved by using low-mass Si beakers as light detectors. These will fully surround the NaI crystal, and thus feature much better light collection efficiency [24] and resolution than the SOS wafer.

VI. CONCLUSIONS

This measurement marks the first proof of event-by-event particle discrimination in a cryogenic NaI detector. We operated a COSINUS prototype with a remoTES sensor, which displayed a baseline resolution of 2.07 keV despite suboptimal, above-ground conditions. It was calibrated with a ^{57}Co γ source and analyzed with a nuclear recoil threshold of 20 keV. Particle discrimination was verified with neutrons from an AmBe source. In Ref. [12], the remoTES design was suggested as an improved readout for delicate absorber materials, which are for example hygroscopic or feature a low melting point. This work shows that the design is indeed suitable for NaI absorbers. The next step in the COSINUS detector optimization strategy in the direction of achieving an energy threshold of 1 keV is an underground measurement with a similar detector, in order to assess its performance in a low-background environment. This measurement has already been performed, and will be the subject of a future publication.

ACKNOWLEDGMENTS

This measurement was possible thanks to the use of the CRESST cryogenic facility and detector production infrastructure at the Max Planck Institute for Physics (MPP). Similarly, the support from the MPP mechanical workshop was invaluable. We thank SICCAS for producing the NaI crystal employed in this measurement. This work has been supported by the Austrian Science Fund FWF, stand-alone project AnaCONDa [P 33026-N], the Austrian Research Promotion Agency (FFG) Project No. ML4CPD, the Research Council of Finland (Grant No. 342777), and the Väisälä foundation.

[1] J. Billard *et al.*, Direct detection of dark matter–APPEC committee report, Rep. Prog. Phys. **85**, 056201 (2022).
[2] R. Bernabei *et al.*, Recent results from DAMA/LIBRA and comparisons, Moscow Univ. Phys. Bull. **77**, 291 (2022).
[3] G. Adhikari *et al.*, Three-year annual modulation search with COSINE-100, Phys. Rev. D **106**, 052005 (2022).
[4] J. Amare *et al.*, Annual modulation results from three-year exposure of ANAIS-112, Phys. Rev. D **103**, 102005 (2021).
[5] D. Cintas, New strategies to improve the sensitivity of the ANAIS-112 experiment at the Canfranc Underground Laboratory arXiv:2310.07339.
[6] D. Cintas *et al.*, Quenching factor consistency across several NaI(Tl) crystals, J. Phys. Conf. Ser. **2156**, 012065 (2021).
[7] M. R. Bharadwaj *et al.*, Quenching factor estimation of Na recoils in NaI(Tl) crystals using a low-energy pulsed neutron beam measurement, SciPost Phys. Proc. **12**, 028 (2023).
[8] M. J. Zurowski, Hidden dependencies in model independent tests of DAMA, SciPost Phys. Proc. **12**, 027 (2023).
[9] J. I. Collar, Quenching and channeling of nuclear recoils in NaI(Tl): Implications for dark-matter searches, Phys. Rev. C **88**, 035806 (2013).
[10] T. Stiegler *et al.*, A study of the NaI(Tl) detector response to low energy nuclear recoils and a measurement of the quenching factor in NaI(Tl), arXiv:1706.07494.
[11] G. Angloher *et al.*, Results from the first cryogenic NaI detector for the COSINUS project, J. Instrum. **12**, P11007 (2017).
[12] G. Angloher *et al.*, First measurements of remoTES cryogenic calorimeters: Easy-to-fabricate particle detectors for a wide choice of target materials, Nucl. Instrum. Methods Phys. Res., Sect. A **1045**, 167532 (2023).
[13] F. Kahlhoefer, F. Reindl, K. Schäffner, K. Schmidt-Hoberg, and Sebastian Wild, Model-independent comparison of annual modulation and total rate with direct detection experiments, J. Cosmol. Astropart. Phys. 05 (2018) 074.
[14] EPO-TEK®, https://www.epotek.com/.
[15] G. Angloher *et al.*, Limits on WIMP dark matter using scintillating $CaWO_4$ cryogenic detectors with active background suppression, Astropart. Phys. **23**, 325 (2005).
[16] Applied Physics Systems, Official website, https://appliedphysics.com/, Accessed: 2023-09-01,
[17] E. Gatti and P. F. Manfredi, Processing the signals from solid-state detectors in elementary-particle physics, Riv. Nuovo Cimento **9**, 1 (1986).
[18] G. Angloher *et al.*, Results on MeV-scale dark matter from a gram-scale cryogenic calorimeter operated above ground, Eur. Phys. J. C **77**, 637 (2017).
[19] F. Pröbst, M. Frank, S. Cooper, P. Colling, D. Dummer, P. Ferger, G. Forster, A. Nucciotti, W. Seidel, and L. Stodolsky, Model for cryogenic particle detectors with superconducting phase transition thermometers, J. Low Temp. Phys. **100**, 69 (1995).

[20] G. Angloher, M. Bauer, I. Bavykina, A. Bento, A. Brown, C. Bucci, C. Ciemniak, C. Coppi, G. Deuter, and F. von Feilitzsch, Commissioning run of the CRESST-II dark matter search, Astropart. Phys. **31**, 270 (2009).
[21] D. Schmiedmayer, Calculation of dark-matter exclusions-limits using a maximum likelihood approach, TU Wien, 2019, 10.34726/hss.2019.63441.
[22] G. Angloher *et al.*, A likelihood framework for cryogenic scintillating calorimeters used in the CRESST dark matter search, arXiv:2403.03824.
[23] G. Angloher *et al.*, Results on low mass WIMPs using an upgraded CRESST-II detector, Eur. Phys. J. C **74**, 1 (2014).
[24] F. Reindl *et al.*, Results of the first NaI scintillating calorimeter prototypes by COSINUS, J. Phys. Conf. Ser. **1342**, 012099 (2020).

Correction: An error in the presentation of the author list was introduced during the proof cycle and has been rectified. Information in the Acknowledgement section has been clarified.